Article

Optical Fibers as Dosimeter Detectors for Mixed Proton/Neutron Fields—A Biological Dosimeter

Jana Niedermeier [1,2,3], Crystal Penner [1], Samuel Usherovich [1], Camille Bélanger-Champagne [1], Elisabeth Paulssen [2,4] and Cornelia Hoehr [1,*]

1 Life Sciences Division, TRIUMF, Vancouver, BC V6T 2A3, Canada
2 Faculty of Chemistry and Biotechnology, FH Aachen, Campus Jülich, 52428 Jülich, Germany
3 Department of Medical Radiation Physics, Carl von Ossietzky University Oldenburg, 26121 Oldenburg, Germany
4 Department Radiation Science and Technology, Technical University Delft, 2629 JB Delft, The Netherlands
* Correspondence: choehr@triumf.ca

Abstract: In recent years, proton therapy has gained importance as a cancer treatment modality due to its conformality with the tumor and the sparing of healthy tissue. However, in the interaction of the protons with the beam line elements and patient tissues, potentially harmful secondary neutrons are always generated. To ensure that this neutron dose is as low as possible, treatment plans could be created to also account for and minimize the neutron dose. To monitor such a treatment plan, a compact, easy to use, and inexpensive dosimeter must be developed that not only measures the physical dose, but which can also distinguish between proton and neutron contributions. To that end, plastic optical fibers with scintillation materials (Gd_2O_2S:Tb, Gd_2O_2S:Eu, and YVO_4:Eu) were irradiated with protons and neutrons. It was confirmed that sensors with different scintillation materials have different sensitivities to protons and neutrons. A combination of these three scintillators can be used to build a detector array to create a biological dosimeter.

Keywords: protons; neutrons; proton therapy; optical fibers; relative dosimetry; Bragg peak; biological dosimeter

1. Introduction

In radiation therapy, tumors or other targeted volumes are treated with ionizing radiation, including photons, electrons, protons, and heavy ions. For a successful treatment, the radiation dose must be high enough to damage the DNA of the cancer cells while being as low as possible to protect the healthy bystander tissue, avoiding side effects. In proton therapy, the spread-out Bragg peak is aligned with the tumor to take advantage of steep dose gradients for a conformal coverage of the tumor and to achieve healthy tissue sparing. As protons travel through beam line elements and the patient towards the tumor, the nuclear interactions of the protons with matter produce secondary neutrons. Neutrons have a higher relative biological effectiveness (RBE) than do protons [1] and could potentially contribute to secondary cancers later in life [2]; however, accounting for neutron dose does not take place during routine treatment planning. Secondary neutrons from the beam line elements can be minimized by active proton delivery, where pencil-beams are scanned by changing the energy of the protons in the accelerator and using steering devices to paint the narrow pencil beam through the target volume. This is in contrast to passive beam delivery, which uses degraders and patient-specific shaping devices upstream of the patient. Active pencil-beam scanning has been shown to reduce the neutron dose to patients [3], but neutron production in the patient cannot be avoided [1,4,5].

Ideally, a treatment plan for a specific patient would not only optimize the proton field overlap with the tumor and minimize the proton exposure to healthy tissue, but also account for and minimize the exposure to secondary neutrons [6]. This can be achieved by

optimizing the treatment angle, treatment energies, and potential boluses for the secondary neutrons. For the quality control (QC) of such a treatment plan before the actual treatment, verification of the neutron dose would be needed, in addition to the proton dose.

Currently, neutrons can be measured with stand-alone detectors, such as a Bonner sphere [7] and a BF_3 proportional counter [8], but the space requirement and data analysis can be cumbersome [6], and due to their size and makeup, they would not be suitable for in vivo measurements. For a QC session in a busy proton therapy center, it would be desirable to have one detector or detector array that is compact, easy to use, efficient, and inexpensive, and which can directly estimate the proportion of the dose attributable to protons and to neutrons in one step—a biological dosimeter that takes the particle type, not just the physical dose, into account.

A detector consisting of two or more optical fiber-scintillator detectors could provide information on neutron and proton contributions to the dose during proton irradiations. Optical fiber-based sensors offer an economical, mm sized potential solution for relative dosimetry, and they are widely studied for this purpose. Studies of scintillators coupled to optical fiber sensors have shown their sensitivity to neutron as well as proton radiation [9–15]. Due to the ease of sealing and waterproofing these sensors, there is also considerable attention given to in vivo applications [16–18].

A detector, built from the combination of scintillation fibers, must meet certain criteria: sufficient light yield for a suitable signal-to-noise ratio; a complementary difference in neutron to proton response to enable the distinguishing of the origin of the deposited dose; small in overall size (1 mm diameter maximum) to provide adequate spatial resolution for measurements in the steep field gradients common in proton therapy; and independence of the signal to the energy of the protons to minimize the effects of quenching along the proton beam axis. This last criterion is especially difficult to fulfill, due to the much-reported effects of quenching in the regions of high linear energy transfer (LET) [19–21]. Quenching refers to an underestimate of the dose deposited due to an alternate mode of energy dissipation. As quenching in many optical fibers is energy dependent and is exhibits a more severe effect for protons at higher LET, this means that the Bragg peak at the end of the proton range appears to be smaller in height than is actually the case. During proton therapy treatment, different energies are applied to provide a homogeneous dose to the extended size of the tumor; thus, a detector which is not energy dependent cannot provide a true dose measurement without corrections.

In this work, the concept of a combined proton/neutron dosimeter is explored by using plastic optical fibers combined with three different scintillator materials (Gd_2O_2S:Tb, Gd_2O_2S:Eu, and YVO_4:Eu). These scintillators were chosen, as they have a large light output and different sensitivities to protons versus neutrons [9].

2. Materials and Methods

2.1. Fibers and Data Acquisition

The optical fiber sensors are made of 1 m long, 1 mm diameter polymethylmethacrylate (PMMA) fibers with a 0.7 mm diameter and 7 mm deep cavities drilled in the end. The cavities, fabricated in the manner of Woulfe et al. [22], are filled with three different inorganic scintillator powders, consisting of A: terbium activated gadolinium oxysulfide (Gd_2O_2S:Tb), B: europium activated gadolinium oxysulfide (Gd_2O_2S:Eu), or C: europium activated yttrium orthovanadate (YVO_4:Eu), see Table 1 and Figure 1. The cavities are sealed with silicone to make the detectors waterproof, and then covered with black tape to block ambient light. The distal ends of the fibers are terminated with SMA 905 connectors and are coupled via SMA-SMA mating sleeves to a PMMA extension, also terminated with an SMA 905 connector. The extension is coupled to a multi pixel photon counter (MPPC) (C11208-350 by Hamamatsu). The MPPC is linked by USB bus directly to a laptop computer where data is viewed in real-time as well as saved as .CSV files for future analysis.

Table 1. Scintillator materials used.

Designation	Scintillator Materials
A	Terbium activated gadolinium oxysulfide, Gd_2O_2S:Tb
B	Europium activated gadolinium oxysulfide, Gd_2O_2S:Eu
C	Europium activated yttrium orthovanadate, YVO_4:Eu
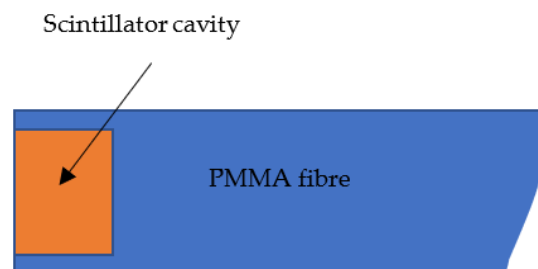
Figure 1. Schematic of the fiber sensor. A 0.7 mm diameter and 0.7 mm deep cavity is drilled into a 1 mm diameter PMMA fiber and filled with scintillator powder; see [22].

When protons or neutrons interact with the scintillator, excitation occurs in the scintillator material. Subsequent decay back to unexcited states results in light output. The emitted photons are then transmitted by the PMMA fibers to the MPPC, and the measured light yield can be related to the deposited dose.

2.2. TRIUMF Proton Therapy Research Center (PTRC) Irradiations

The proton irradiations were carried out at the Proton Therapy Research Center (PTRC) at TRIUMF. The TRIUMF main cyclotron, capable of delivering protons with a maximum energy of 520 MeV, provides 74 MeV protons to the PTRC facility for these experiments at a current of 2 nA. The facility was in clinical use to treat choroidal melanomas from 1995 to 2019 [23,24]. The proton beam enters the treatment room and traverses a lead disk which serves the functions of primary collimator and scatterer (Figures 2 and 3). The 0.8 mm thick disk spreads the beam to a useful and repeatable size—over several cm in diameter—for experiments and treatments. Next, the beam passes through a range shifter, to change the proton energy according to its maximum desired range, and a modulator wheel, which is a rotating disk with different thicknesses, to generate a Spread-Out Bragg Peak (SOBP) of 23 mm in depth. After that, the beam passes through a second collimator, an ion chamber, to monitor the delivered dose during irradiation, and the PT nozzle, with a 25 mm diameter collimator. Behind the PT nozzle is a water phantom with an entry window of 1 mm thick solid water. The optical fiber to be tested is placed behind the solid water window in the water box and is attached to a remote-controlled 3D stage which precisely controls the position of the fiber.

2.2.1. PTRC Depth Dose Measurements

To measure the depth dose, the fiber is scanned axially from just behind the solid water window (0 mm axial depth) to past the end of the Bragg peak (45 mm axial depth). The stage pauses in 0.79 mm steps for a set amount of dose, as measured by the ion chamber in monitor counts (MC). The light output of the fiber is recorded at each position. This axial profile is then compared to our standard calibration detector, a Markus chamber (a parallel plate ionization chamber), for the assessment of the sensor response in varying LET conditions along the depth dose.

To measure the relative sensitivity of the three fibers A, B, and C in a proton field, each fiber was placed in a reference position P in the plateau of the SOBP; see Figure 5. The transversal position in the center of the beam is determined using laser markers mounted in the room.
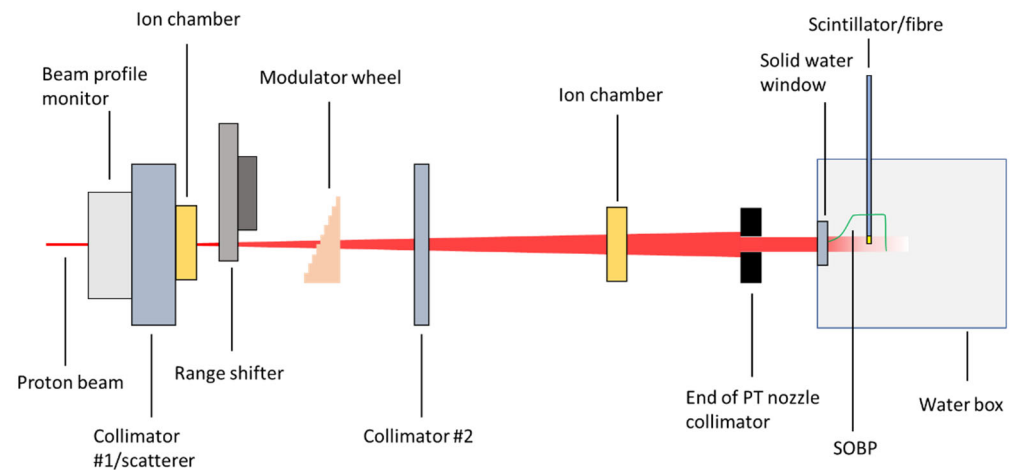
Figure 2. Simplified drawing of the experiment setup at the PTRC. The beam from the main cyclotron enters from the left and passes a collimator/scatterer, a range shifter, a range modulator, a second collimator, and an ion chamber to monitor the beam during delivery; then the beam traverses the PT nozzle, including a final collimator, and stops in the water phantom, where the fiber is mounted on a 3D stage.
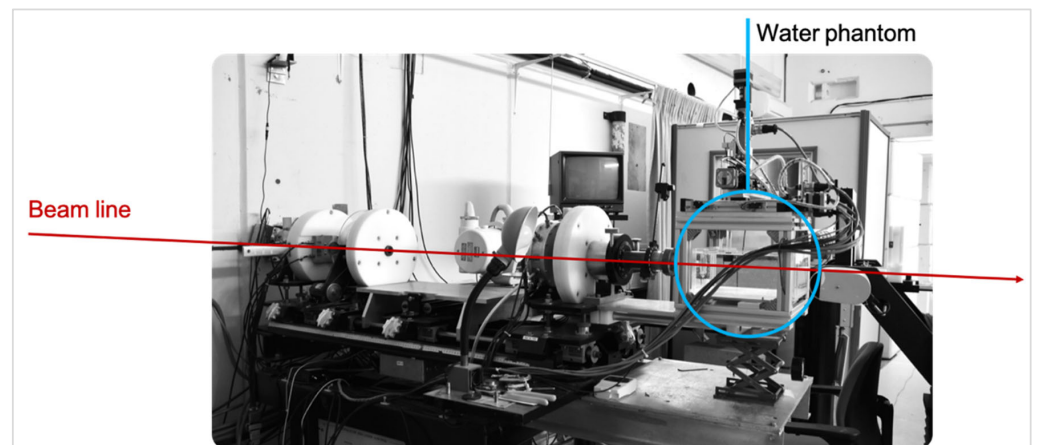

Figure 3. Photo of the experimental setup at the PTRC. The water phantom in which the fibers are placed is highlighted in blue and the beam axis in red.

2.2.2. PTRC Sensitivity Measurements

The relative proton sensitivity of the sensors was found by measuring the light output response of each scintillator three times in the reference position for 10,000 MC (140 cGy) irradiations. The cumulative background signal before beam delivery was averaged and subtracted from each data point (one point every 0.1 s), and then the total signal was summed for the duration of the trial. The exact amount of delivered MC varied per experiment; therefore, the total cumulative signal was divided by the MC delivered. For the sensitivity comparison, the mean value of the three trials was found, and the standard deviation among the three was calculated.

At the PTRC, the proton field is mixed with a small number of secondary neutrons due to interactions of the protons with beam line elements and the water box. The proportion of neutrons in the reference position at the PTRC without an energy shift and the 23 mm modulator wheel amounts to 3.5% of the proton dose, as determined by Monte Carlo simulations that were performed with the FLUKA package in previous work and validated with BF_3 counters [6].

The light spectrum under proton irradiation was measured in the reference condition with a SM442-URN010-USB spectrometer (Spectral Products, Putnam, Oklahoma, USA) for spectral comparison.

2.3. TRUMF Neutron Facilty (TNF) Measurements

Neutron irradiations were carried out at the TRIUMF Neutron Facility (TNF) to determine the relative fiber sensitivities to the neutrons. After traversing the beam line 1A, 480 MeV protons are stopped in a beam dump on an aluminum absorber surrounded by a water modulator. Here, neutrons are created via spallation reactions. Some of these neutrons reach the TNF facility, where a 5 cm by 15 cm neutron field is accessible by a 5 m vertical channel. The beam is actively monitored via a neutron detector, and over the course of these experiments, the neutron flux measured was $(8.3 \pm 0.2) \times 10^6$ n/(cm^2 s), where n is the number of neutrons with an energy greater than 0.1 MeV. This corresponds to a dose rate of $(3.2 \pm 0.6) \times 10^{-4}$ Gy/s.

TNF Sensitivity Measurements

To measure the relative neutron sensitivity of our fibers, the sensor ends were attached to an aluminum board. Each measurement consisted of lowering the one sensor on the board down the channel until the sensor was in the neutron field center. The sensor was left in place for approximately 20 s, and the neutron dose measurement downstream of the sensor apparatus was recorded for the period before, during, and after the fiber was inserted into the beam. The small fluctuations in neutron flux at TNF were accounted for by dividing the fiber counts (FC) by the average neutron monitor counts (NMC) measured before and after each irradiation. The assembly was then raised out of the field long enough to ensure that light decay was occurring, then lowered back in for a total of three measurements.

Relative neutron sensitivity was determined by subtracting an average background from each of the three trials, then dividing the summed signal over the course of the irradiation and dividing it by the time it took, in seconds. Dividing the signal by the duration of the irradiation was necessary due to each trial being of slightly different lengths, since the raising and lowering of the sensors is fully manual, and there can be one to two seconds difference in the trial duration. The normalized signal/second was then divided by the signal rate determined by the neutron detector found behind the sensing apparatus over the course of the irradiation. The three trials for each individual sensor were then averaged, and the standard deviation between trials was calculated and compared. A comparison of relative neutron sensitivities is seen in Table 2.

Table 2. MPPC signal with standard deviation per scintillator output for protons and neutrons. The highest signal (shown in bold) among the sensors was used to normalize all three.

Sensor	Protons	Neutrons
Gd$_2$O$_2$S:Tb (A)	0.57 ± 0.03	**1.00** ± 0.01
Gd$_2$O$_2$S:Eu (B)	0.952 ± 0.008	0.241 ± 0.002
YVO$_4$:Eu (C)	**1.000** ± 0.002	0.412 ± 0.003

2.4. Equations

Under reference conditions, formulae for the light yield *N* and sensitivity *S* as a function of the dose delivered by the protons and neutrons in water are detailed in Equations (1)–(5).

The light yield N_{TNF}^x of a fiber x at the TNF deposited by neutrons of dose D_{PT}^n is

$$N_{TNF}^x = S_n^x \cdot D_{TNF}^n \qquad \text{with } D_{TNF}^n = n_{TNF} \cdot d_{TNF} \qquad (1)$$

The light yield N_{PT}^x of a fiber x at the PTRC with proton dose D_{PT}^p and neutron dose D_{PT}^n is

$$N_{PT}^x = S_p^x \cdot D_{PT}^p + S_n^x \cdot D_{PT}^n \qquad \text{with } D_{PT}^p = p \cdot d_{PT} \tag{2}$$

Therefore, the sensitivity of fiber x to neutrons at TNF is

$$S_n^x = \frac{N_{TNF}^x}{D_{TNF}^n} \tag{3}$$

and the sensitivity of fiber x to protons at PTRC is

$$S_p^x = \frac{N_{PT}^x}{D_{PT}^p} - \frac{D_{PT}^n}{D_{PT}^p} \cdot S_n^x \tag{4}$$

where the relative neutron to proton dose under reference conditions is given by $\frac{D_{PT}^n}{D_{PT}^p}$ (at point P) = 0.035, leading to a final value for the sensitivity to protons of:

$$S_p^x = \frac{N_{PT}^x}{D_{PT}^p} - 0.035 \cdot S_n^x \tag{5}$$

with light yield (N) measured in fiber counts (FC) and $N_{PT}^x[FC]$—light yield of fiber x at PTRC under reference conditions, $N_{TNF}^x[FC]$—light yield of fiber x at TNF, $S_p^x\left[\frac{FC}{cGy}\right]$—sensitivity of fiber x to protons, $S_n^x\left[\frac{FC}{cGy}\right]$—sensitivity of fiber x to neutrons, $p[MC]$—proton fluence at PIF measured in monitor counts (MC), $D_{PT}^p[cGy]$—proton dose at PTRC under reference condition, $n_{TNF}[NMC]$—neutron fluence at TNF measured in neutron monitor counts (NMC), $D_{TNF}[cGy]$—neutron dose to water at TNF, $n_{PT}[NMC]$—secondary neutron fluence at PTRC, $D_{PT}^n[cGy]$—secondary neutron dose to water at PTRC, $d_{PT}\left[\frac{cGy}{MC}\right]$—dose per MC at PTRC, and $d_{TNF}\left[\frac{cGy}{NMC}\right]$—dose per NMC at TNF.

After the fiber sensitivities in the reference position are determined, an SOBP beam of unknown relative proton and neutron composition can be characterized using two different scintillating fibers. The light yields x of fiber A and B in unknown (u) beam composition at PTRC with the sensitivities determined from Equations (3) and (5) are

$$x_A = S_n^A n_u + S_p^A p_u \tag{6}$$

$$x_B = S_n^B n_u + S_p^B p_u \tag{7}$$

Therefore, the proton dose at PTRC is

$$p_u = \frac{x_A S_n^B - x_B S_n^A}{S_p^A S_n^B - S_p^B S_n^A} \tag{8}$$

and the neutron dose at PTRC is:

$$n_u = \frac{x_A S_p^B - x_B S_p^A}{S_n^A S_p^B - S_n^B S_p^A} \tag{9}$$

From these, a neutron-to-proton ratio R of the dose delivered can be obtained with

$$R = \frac{n_u}{p_u} = \frac{x_B S_p^A - x_A S_p^B}{x_A S_n^B - x_B S_n^A} \tag{10}$$

where the expected ratio is 0.035 at the reference position and $x_A[FC]$—light yield of fiber A along the SOBP at PTRC, $x_B[FC]$—light yield of fiber B along the SOBP at PTRC, $p_u[cGy]$—

proton dose along the SOBP at PTRC, $n_u[cGy]$—neutron dose along the SOBP at PTRC, and R—neutron-to-proton ratio along the SOBP at PTRC.

If three or more fibers are used instead of only two, we can obtain additional neutron-to-proton ratios based on different scintillator combinations, which can be averaged and the standard deviation found. Averaging multiple ratios based on different combinations of scintillators increases the likelihood of estimating the true neutron-proton dose ratio.

3. Results and Discussion

3.1. Proton Results—Depth Dose

Figure 4 show the Bragg peak normalized to the dose at the entrance, as measured by the Markus chamber and the three sensors A, B, and C. The Markus chamber is considered the gold standard for the measurement of proton beams and at the PTRC at TRUMF, the ratio from the entrance to the peak is 3.7, but the entrance to the peak ratio of sensor A is 3.0, for sensor B, it is 2.7, and for sensor C, it is 2.9. All three clearly underestimate the dose deposited at the low energy in the Bragg peak, which coincides with the highest LET. This quenching has been identified previously [9,21], and it demonstrates an energy dependence of the three sensors. In principle, this energy dependence can be corrected via the Birks' equation [13,25].
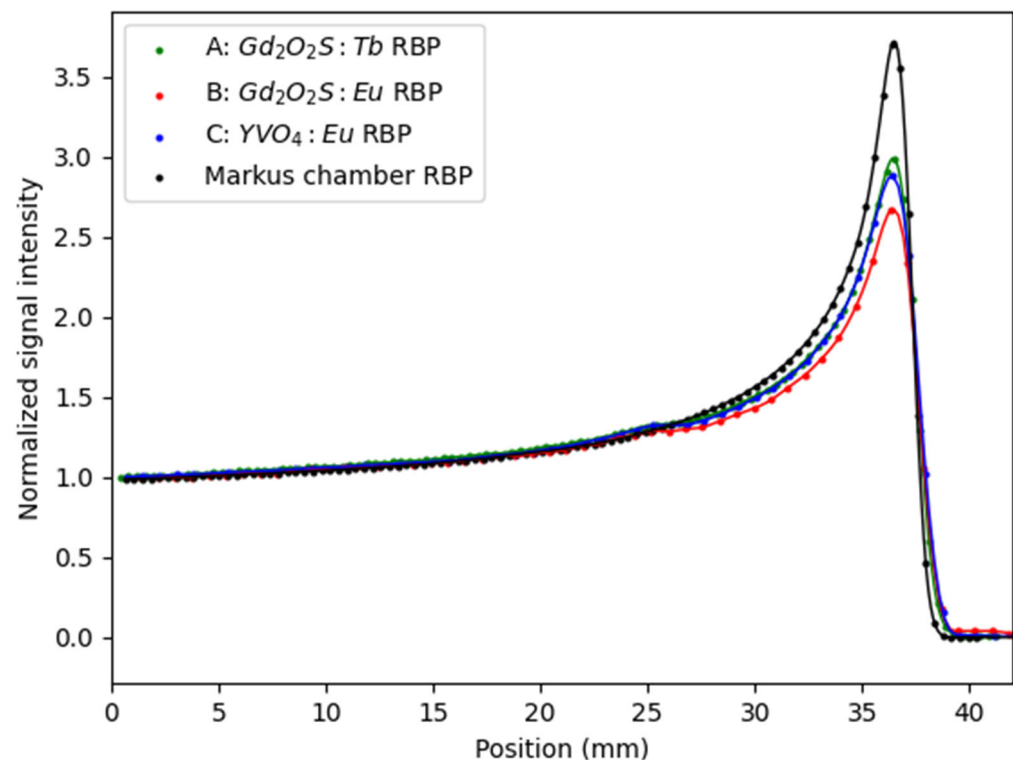

Figure 4. Raw Bragg peaks of the three scintillators and the Markus chamber, normalized at the entrance at position 0 mm. Positions were shifted to align the peaks. Peak-to-entrance ratios of scintillators A, B, C, and the Markus chamber from the interpolated B-splines are 3.0, 2.7, 2.9, and 3.7, respectively.

Each of the three scintillators was scanned through the 23 mm SOBP and compared in Figure 5 to the Markus chamber measurement. The Markus chamber is considered the gold standard for measuring proton beams. The three fibers do have a significant slope and decrease towards the distal end of the SOBP, as all three scintillators exhibit quenching at higher LET at the distal end of the SOBP.
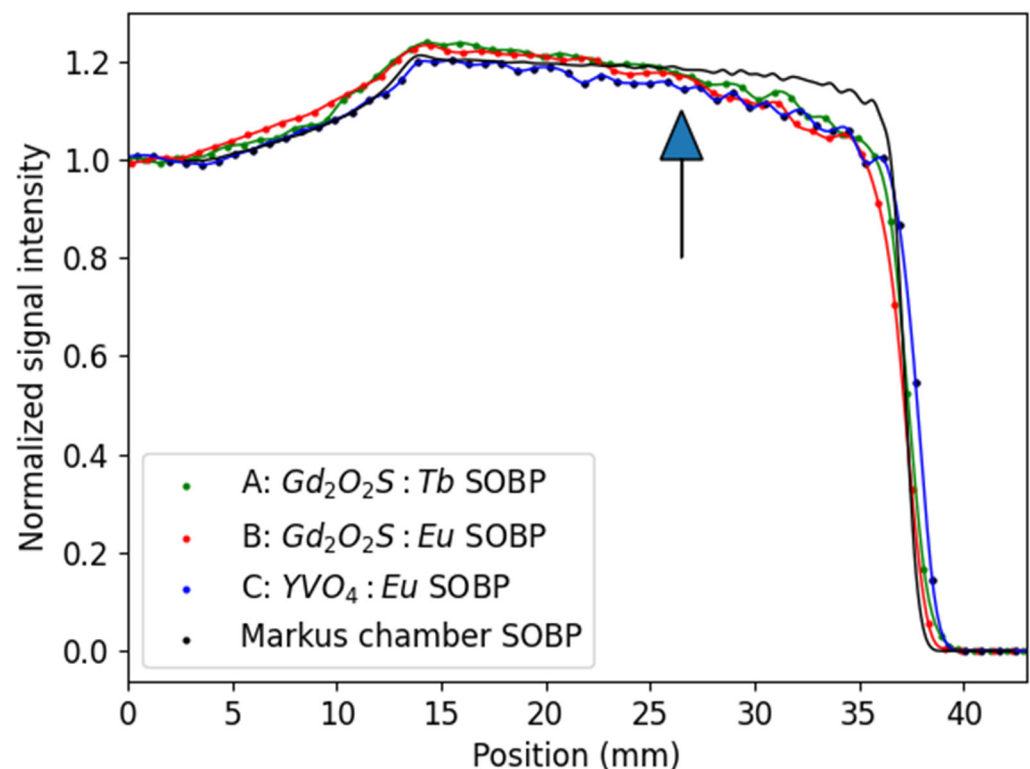
Figure 5. The 23 mm SOBPs for the three scintillators as compared to those of the Markus chamber, normalized at the entrance by setting the average of the first 5 data points to 1. All three scintillators experience quenching at the distal end of the plateau when compared with the Markus chamber. The arrow points to the reference position. The solid lines are interpolated B-splines.

3.2. Proton and Neutron Sensitivity

Normalized sensitivity comparisons are found in Table 2, normalized to the highest sensitivity for protons and neutrons. The highest sensitivity to protons among the scintillators is (C), the middle is (B), and the lowest is (A). In contrast, sensor (A) has the highest sensitivity to neutrons, the middle is (C) and the lowest is (B). A graphical presentation is shown in Figure 6. Based on these results, a combination of sensors (A) and (B) or (A) and (C) will make it possible to distinguish between the proton and neutron dose, making them a good match, considering our criterion for complementary sensitivities to the two particles.

Based on the sensitivities found in the previous section, Equations (3) and (5) result in the sensitivities summarized in Table 3.

Table 3. Scintillator sensitivities.

Scintillator	Sensitivity to Protons (FC/cGy)	Sensitivity to Neutrons (FC/cGy)
Gd_2O_2S:Tb (A)	$(500 \pm 30) \times 10^3$	$(1087 \pm 8) \times 10^3$
Gd_2O_2S:Eu (B)	$(846 \pm 7) \times 10^3$	$(265 \pm 2) \times 10^3$
YVO_4:Eu (C)	$(889 \pm 2) \times 10^3$	$(449 \pm 4) \times 10^3$

3.3. PTRC Spectrum Measurements

Figure 7 shows the wavelength measuements of the three sensors under proton irradiation in the reference position. While the spectra of sensors (A) and (C) are very similar, with smaller peaks at 490 nm and 580 nm, and a larger peak at 550 nm, sensor (B) exhibits an overlapping peak at 590 nm, but a different peak at 625 nm. This feature would allow for additional discrimination between the proton and neutron doses in a two-step process, even if only one photon detector is used: if the light of sensors (A) (or (C)) and (B) are

combined and sent to a detector in a first step, and if a long-pass filter is inserted that allows light to transmit only above 610 nm in a second step, the first step will mesure the light output from both sensor (A) and (B), while the second step will only measure the light output of sensor (B). Togther with the sensitivities from Equations (3) and (5), the contributions from protons and neutrons can be determined.
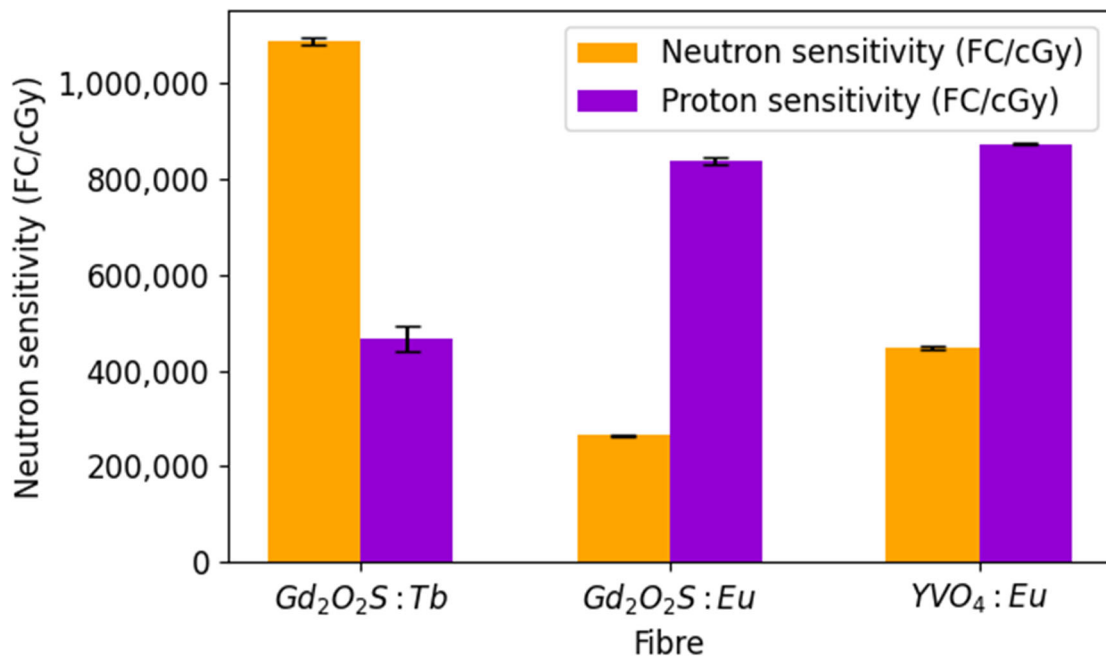

Figure 6. Comparison of sensor sensitivities to protons (orange) and neutrons (purple), averaged over 3 measurements. Black error bars indicate the calculated standard deviation of the measurements.
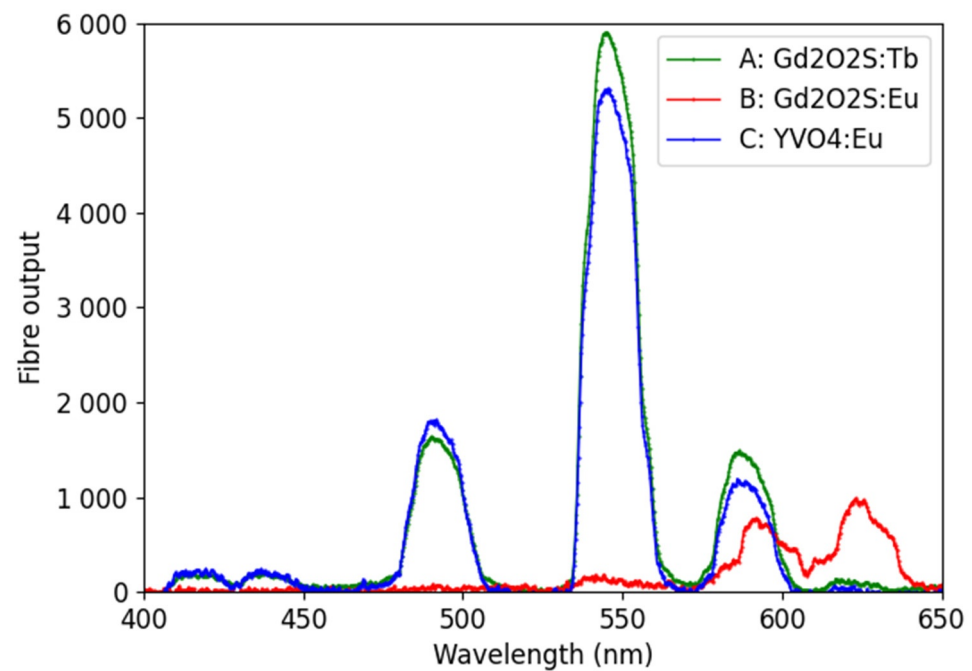

Figure 7. Spectrometer data for the three sensors under proton irradiation in the reference condition.

4. Summary and Outlook

The measurements in this work are in agreement with our previous findings of individual sensors [9] and confirm that the scintillators have varying responses between protons

and neutrons: Gd_2O_2S:Tb (A) is more sensitive to neutrons than to protons, and Gd_2O_2S:Eu (B) and YVO_4:Eu (C) are more sensitive to protons than to neutrons. By combining the three sensors into a single array and placing them into a mixed proton/neutron field, the different responses of the sensors will give an estimation of the doses from the different particle types, once calibrated with Equation (10).

All three tested scintillators do exhibit a non-linear response to increasing LET, or quenching. This under-response in an absorbed dose will have to be corrected for in a future prototype in order to report the physical dose deposited. Future studies will incorporate organic scintillators, for which corrections are possible via Birks' quenching equation [25], that, in combination with the scintillators described here, will increase the accuracy of proton to neutron ratios.

Author Contributions: Conceptualization, C.H. and C.P.; methodology, J.N., C.P., S.U. and C.H.; software, J.N., C.P. and S.U.; validation, J.N., C.P. and S.U.; formal analysis, J.N., C.P., S.U. and C.H.; investigation, J.N., C.B.-C. and C.P.; resources, C.H. and C.B.-C.; data curation, J.N., C.P. and S.U.; writing—original draft preparation, J.N., C.P., S.U. and C.H.; writing—review and editing, all; visualization, J.N., C.P. and S.U.; supervision, C.H. and E.P.; project administration, C.H. and E.P.; funding acquisition, C.H. All authors have read and agreed to the published version of the manuscript.

Institutional Review Board Statement: Not applicable.

Informed Consent Statement: Not applicable.

Data Availability Statement: Not applicable.

Conflicts of Interest: The authors declare no conflict of interest.

References

1. Hälg, R.A.; Schneider, U. Neutron dose and its measurement in proton therapy—Current state of knowledge. *Br. J. Radiol.* **2020**, *93*, 20190412. [CrossRef] [PubMed]
2. Dell'Oro, M.; Short, M.; Wilson, P.; Peukert, D.; Hua, C.-H.; Merchant, T.E.; Bezak, E. Lifetime attributable risk of radiation induced second primary cancer from scattering and scanning proton therapy–A model for out-of-field organs of paediatric patients with cranial cancer. *Radiother. Oncol.* **2022**, *172*, 65–75. [CrossRef] [PubMed]
3. Rasouli, F.S. A Monte Carlo simulation study on the secondary neutron dose in passive proton therapy. *Radiat. Phys. Eng.* **2022**, *3*, 33–38.
4. Fontenot, J.; Taddei, P.; Zheng, Y.; Mirkovic, D.; Jordan, T.; Newhauser, W. Equivalent dose and effective dose from stray radiation during passively scattered proton radiotherapy for prostate cancer. *Phys. Med. Biol.* **2008**, *53*, 1677. [CrossRef] [PubMed]
5. Azadegan, N.; Hassanpour, M.; Khandaker, M.U.; Iqbal Faruque, M.R.; Al-mugren, K.S.; Bradley, D.A. Calculation of secondary radiation absorbed doses due to the proton therapy on breast cancer using MCNPX code. *Radiat. Phys. Chem.* **2021**, *183*, 109427. [CrossRef]
6. Lindsay, C.D. Simulation of the TRIUMF Proton Therapy Facility for Applications to 3D Printing in Radiotherapy. Ph.D. Thesis, University of Victoria, Victoria, BC, Canada, 2021.
7. Awschalom, M.; Sanna, R.S. *Applications of Bonner Sphere Detectors in Neutron Field Dosimetry*; Fermi National Accelerator Lab.: Batavia, IL, USA, 1983.
8. Andersson, I.Ö.; Braun, J. *A Neutron Rem Counter*; Aktiebolaget Atomenergi: Stockholm, Sweden, 1964.
9. Penner, C.; Woulfe, P.; Stoeber, B.; Duzenli, C.; O'Keeffe, S.; Hoehr, C. Novel optical fibre-based sensors for neutron and proton beams. In Proceedings of the 2019 IEEE SENSORS, Montreal, QC, Canada, 27–30 October 2019; pp. 1–4. [CrossRef]
10. Ishikawa, A.; Yamazaki, A.; Watanabe, K.; Yoshihashi, S.; Uritani, A.; Tsurita, Y.; Tsuchida, K.; Kiyanagi, Y. A comparison between simulation and experimental results for depth profile of 6Li reaction rate in a water phantom of BNCT using a small 6Li-based scintillator neutron detector with an optical fiber. *Radiat. Meas.* **2020**, *133*, 106270. [CrossRef]
11. Savard, N.; Penner, C.; Dehnel, M.; Potkins, D.; Hoehr, C. *Characteristics of a Ce-Doped Silica Fiber Irradiated by 0–400 MeV Neutrons*; IEEE: Piscataway, NJ, USA, 2018.

12. Kim, S.H.; Lee, J.W.; Jung, W.S.; Ahn, J.K.; Jung, M.H.; Kim, Y.J. Three-dimensional measurement of a proton beam profile at KOMAC with a scintillating fiber detector. *Nucl. Instrum. Methods Phys. Res. Sect. A Accel. Spectrometers Detect. Assoc. Equip.* **2022**, *1034*, 166832. [CrossRef]

13. Hoehr, C.; Lindsay, C.; Beaudry, J.; Penner, C.; Strgar, V.; Lee, R.; Duzenli, C. Characterization of the exradin W1 plastic scintillation detector for small field applications in proton therapy. *Phys. Med. Biol.* **2018**, *63*, 095016. [CrossRef] [PubMed]

14. Archambault, L.; Polf, J.C.; Beaulieu, L.; Beddar, S. Characterizing the response of miniature scintillation detectors when irradiated with proton beams. *Phys. Med. Biol.* **2008**, *53*, 1865. [CrossRef] [PubMed]

15. Safai, S.; Lin, S.; Pedroni, E. Development of an inorganic scintillating mixture for proton beam verification dosimetry. *Phys. Med. Biol.* **2004**, *49*, 4637. [CrossRef] [PubMed]

16. Woulfe, P.; Sullivan, F.; Kam, W.; O'Keeffe, S. Optical fiber dosimeter for real-time in-vivo dose monitoring during LDR brachytherapy. *Biomed. Opt. Express* **2020**, *11*, 4027–4036. [CrossRef] [PubMed]

17. Jørgensen, E.B.; Johansen, J.G.; Overgaard, J.; Piché-Meunier, D.; Tho, D.; Rosales, H.M.; Tanderup, K.; Beaulieu, L.; Kertzscher, G.; Beddar, S. A high-Z inorganic scintillator–based detector for time-resolved in vivo dosimetry during brachytherapy. *Med. Phys.* **2021**, *48*, 7382–7398. [CrossRef] [PubMed]

18. Cometti, S.; Gierej, A.; Giaz, A.; Lomazzi, S.; Baghdasaryan, T.; Van Erps, J.; Berghmans, F.; Santoro, R.; Caccia, M.; O'Keeffe, S. Characterization of scintillating materials in use for brachytherapy fiber based dosimeters. *Nucl. Instrum. Methods Phys. Res. Sect. A Accel. Spectrometers Detect. Assoc. Equip.* **2022**, *1042*, 167083. [CrossRef]

19. Ding, L.; Wu, Q.; Wang, Q.; Li, Y.; Perks, R.M.; Zhao, L. Advances on inorganic scintillator-based optic fiber dosimeters. *EJNMMI Phys.* **2020**, *7*, 1–23. [CrossRef]

20. Hirata, Y.; Watanabe, K.; Yoshihashi, S.; Uritani, A.; Koba, Y.; Matsufuji, N.; Yanagida, T.; Toshito, T.; Fukuda, K. Particle dependence of quenching effect in an optical-fiber-type optically stimulated luminescence dosimeter. *Sens. Mater.* **2017**, *29*, 1455–1464.

21. Hoehr, C.; Penner, C.; O'keeffe, S.; Woulfe, P.; Capoen, B.; El Hamzaoui, H.; Bouwmans, G.; Morana, A.; Girard, S. Optical Fibers for Dosimetry in External Beam Therapy. In *Optical Sensors and Sensing Congress*; Optica Publishing Group: Washington, DC, USA, 2020; p. STu5D.2. [CrossRef]

22. Woulfe, P.; Sullivan, F.J.; Byrne, L.; Doyle, A.; Kam, W.; Martyn, M.; O'Keeffe, S. Optical fibre based real-time measurements during an LDR prostate brachytherapy implant simulation: Using a 3D printed anthropomorphic phantom. *Sci. Rep.* **2021**, *11*, 1–8. [CrossRef]

23. Tran, E.; Ma, R.; Paton, K.; Blackmore, E.; Pickles, T. Outcomes of proton radiation therapy for peripapillary choroidal melanoma at the BC Cancer Agency. *Int. J. Radiat. Oncol. Biol. Phys.* **2012**, *83*, 1425–1431. [CrossRef] [PubMed]

24. Blackmore, E.; Evans, B.; Mouat, M. Operation of the TRIUMF proton therapy facility. In Proceedings of the 1997 Particle Accelerator Conference (Cat. No. 97CH36167), Vancouver, BC, Canada, 12–16 May 1997; pp. 3831–3833.

25. Birks, J. *The Theory and Practice of Scintillation Counting*; International Series of Monographs in Electronics and Instrumentation; Elsevier: Amsterdam, The Netherlands, 1964; ISBN 9781483156064.